Phase Equilibria in the Sodium Fluoride Enriched Region of the Reciprocal System Na_6F_6–Al_2F_6–Na_6O_3–Al_2O_3

PERRY A. FOSTER, Jr.
Aluminum Company of America, New Kensington, Pa.

The location of univariant lines and invariant points in the sodium fluoride enriched region of the Na_6F_6–Al_2F_6–Na_6O_3–Al_2O_3 reciprocal system were determined by refractive index and x-ray diffraction measurements of quenched samples. Two peritectic reaction points and one eutectic are defined.

The cryolite-sodium aluminate section is taken from the reciprocal diagram and plotted as conventional molar quantities. The section is shown to lack the qualities of a true system since β-alumina (the composition point of which is not located on the join) precipitates as primary phase.

THE RECIPROCAL system, Na_6F_6–Al_2F_6–Na_6O_3–Al_2O_3 has been studied by Kostjukov (*11*). The planar square plot indicates that a univariant line separates the sodium fluoride and sodium aluminate phase fields in the NaF-rich region of the diagram. This line terminates at a peritectic invariant point where β-alumina also precipitates.

Recently published works on the NaF–Al_2O_3 system (*8, 9*) agree that this is the case, but the composition of the peritectic is at a much lower alumina content. Two other univariant lines originating at the cryolite-sodium fluoride and at the cryolite-alumina binary eutectics are shown by Kostjukov to join at an invariant eutectic point where the melt is triply saturated with respect to cryolite, β-alumina and sodium fluoride. The line joining the cryolite composition point at the 1:1 Na_6F_6/Al_2F_6 ratio and the Al_2O_3 corner of the diagram is said to separate the α- and β-Al_2O_3 phase fields. If that part of the cryolite-alumina join which cuts across the alumina phase field represents univariant equilibrium between α-Al_2O_3, β-Al_2O_3 and liquid, it couldn't possibly terminate at the alumina corner. For many years β-Al_2O_3 was thought to be a metastable polymorph of corundum. In this event, an isotherm would likely separate the two fields rather than an univariant line. The work of DePable-Galan (*5*) in the Na_2O–Al_2O_3–SiO_2 system refutes the notion of polymorphism and assigns a stable composition point to β-Al_2O_3($Na_2O \cdot 11Al_2O_3$) on the Na_2O–Al_2O_3 axis with eutectic points on both sides of the vertex. The α-Al_2O_3–β-Al_2O_3 eutectic thus defined provides a terminus (that satisfies the phase rule) for the univariant line involving these phases rather than the alumina corner. However, if the view that the cryolite-alumina tie line separates the α- and β-Al_2O_3 phase fields further in the diagram is valid, then the cryolite-alumina system doesn't possess a simple eutectic. A reaction point (peritectic) must exist at the minimum of the two intersecting liquidus curves where the three solid phases α-Al_2O_3, β-Al_2O_3 and cryolite can exist in equilibrium with the liquid phase. Recent papers describing the phase relationships in the cryolite-alumina system (*4, 7, 14*) show conclusively that this is not the case. The publications of Albert and Breit (*1*), Pazukhin (*12*) and Arakelyan (*2*) report the identification of β-Al_2O_3 in basic cryolite-alumina melts. A peritectic reaction point is expected, if not on the cryolite-alumina join, then certainly on the sodium fluoride enriched side of that line. Phillips (*13*) gives liquidus isotherms on a Na_3AlF_6–NaF–Al_2O_3 ternary plot, which indicate a peritectic close to the Na_3AlF_6–Al_2O_3 binary ordinate. The experimental technique employed to determine these liquidus temperatures precludes identifying the equilibrium solid phases. The location of a ternary eutectic, however, is absent.

This paper gives the results of applying the quenching method to the determination of liquidus temperatures for several sodium fluoride isocomposition sections and selected composition points in the Na_3AlF_6–NaF–Al_2O_3 triangle. The weight % concentration terms employed in relation to the experimentally determined liquidus temperatures (Figures 1 and 2) and the subsequent location of phase fields in the composition triangle (Figure 3) are converted to reciprocal Na_6F_6–Al_2F_6–Na_6O_3–Al_2O_3 quantities, facilitating the tracing of crystallization paths (Figure 4).

EXPERIMENTAL

Details of the quenching procedure and the microscopy techniques used in the study of the quenched sample are essentially the same as described in a previous publication (*6*).

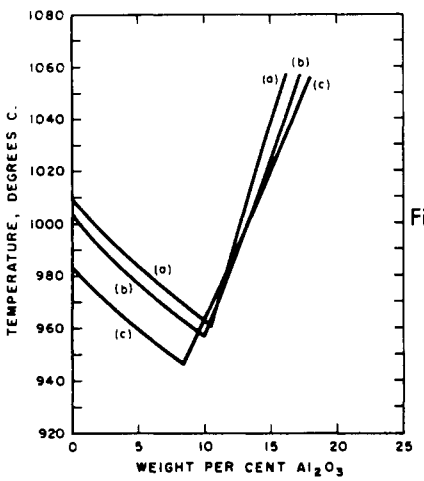

Figure 1. Liquidus curves;
(a) Na_3AlF_6–Al_2O_3
(b) 5 wt. % NaF section
(c) 15 wt. % NaF section

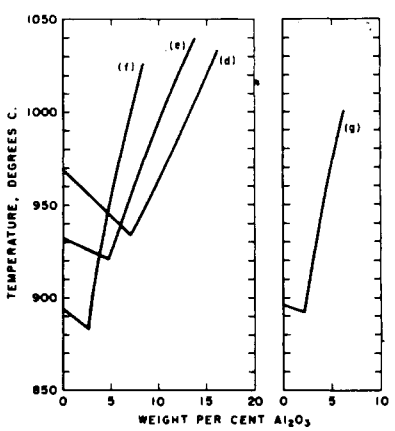

Figure 2. Liquidus curves; NaF sections,
(d) 20 wt. %
(e) 30 wt. %
(f) 40 wt. %
(g) 42 wt. %

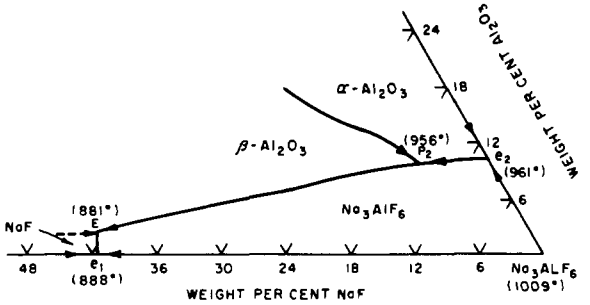

Figure 3. Location of phase fields in the cryolite corner of the Na_3AlF_6–NaF–Al_2O_3 composition triangle

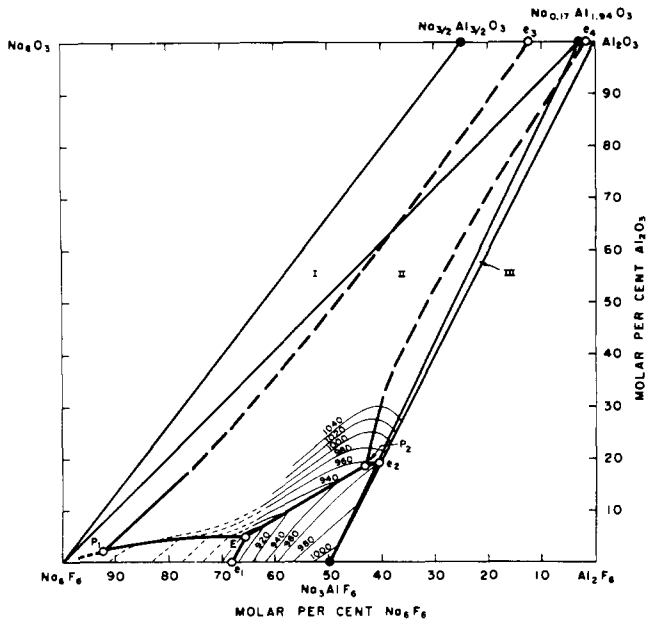

Figure 4. The reciprocal system Na_6F_6–Al_2F_6–Na_6O_3–Al_2O_3

Pt, Pt-10% Rh thermocouples were used to determine quenching temperatures. Calibration was based on an e.m.f. versus temperature curve employing the following fixed points: gold (wire), 1063°; Na_2SO_4, 884.8° and NaCl, 800.5° C.

Hand-picked, Greenland cryolite was used. The impurities were silicon (SiO_2), 0.14%; potassium (KF), 0.005%; calcium (CaF_2), 0.01%; and lithium (LiF), 0.035%. Sodium fluoride was certified by the Fisher Scientific Company as having the following impurities: iron, 0.002%; heavy metals as lead, 0.003%; water insoluble matter, 0.005%. The alumina used was Alcoa's A-14 grade. Predominant impurities in this material are soda, 0.092% and silica, 0.19%.

Ternary compositions low in sodium fluoride and alumina were prefused in a platinum crucible under argon, ground to pass 100-mesh size screen, homogenized by mechanical mixing and dried. Ten to fifteen milligrams was then charged into small platinum tubes and sealed. Other compositions, high in sodium fluoride and alumina, were weighed directly in the platinum tubes.

The identity of the precipitating primary phase particles (Na_3AlF_6, NaF, β-Al_2O_3, α-Al_2O_3 and $NaAlO_2$) was determined by refractive index measurements and x-ray powder diffraction.

RESULTS AND DISCUSSION

The shape of the primary phase surfaces, the location of univariant lines, and the invariant points in the cryolite rich end of the Na_3AlF_6–NaF–Al_2O_3 composition triangle were determined from the liquidus temperatures for the following NaF sections: 5, 15, 20, 30, 40 and 42 wt. %.

The liquidus curves for the 5 wt. % (b) and 15 wt. % (c) NaF sections and those of the cryolite-alumina system (a) are shown in Figure 1. The cryolite freezing point is depressed uniformly towards a minimum with increasing alumina content. The minimum represents a composition and temperature where the melts of a given section are doubly saturated with respect to cryolite and alumina. Each minimum defines a point of intersection with the ternary univariant line that originates at the cryolite-alumina eutectic.

As can be seen from Figure 1, the addition of NaF displaces the minimum toward lower alumina. At higher alumina contents than the double saturation point, the primary phase is alumina or an aluminate depending on the NaF content. System (a) and section (b) precipitate α-Al_2O_3. Section (c), however, precipitates β-Al_2O_3 as primary phase for compositions containing 8.4–17 wt. % alumina. Quenches of samples containing 18 wt. % alumina precipitate α-Al_2O_3. The 15 wt. % NaF section cuts across α-, β-Al_2O_3 univariant line at high alumina contents (17–18 wt. %).

Several composition points were investigated to locate the α-, β-Al_2O_3 univariant line. Table I lists those that were helpful in defining that line and its inter-section with the cryolite-alumina univariant. A peritectic reaction point was located at 6.6 wt. % NaF, 9.9 wt. % Al_2O_3 and 83.5 wt. % Na_3AlF_6, Figure 3, where α-Al_2O_3, β-Al_2O_3 and Na_3AlF_6 solid phases exist in equilibrium with liquid phase at 956°. Before the temperature can be reduced, the reaction

$$\text{Liquid} + \alpha\text{-}Al_2O_3 = \beta\text{-}Al_2O_3 + Na_3AlF_6$$

must progress to the complete consumption of α-Al_2O_3.

Figure 1 shows that the slope of the alumina liquidus decreases with increasing NaF content. As a consequence, addition of NaF increases the solubility of Al_2O_3 at high temperatures although the converse is true at low temperatures. For example at 970°, a melt containing cryolite and 15 wt. % NaF dissolves 10.6 wt. % Al_2O_3; whereas cryolite alone dissolves 11.1 wt. % Al_2O_3 at this temperature. However, at 1050° C. a cryolite-15 wt. % NaF melt can dissolve 17.5 wt. % Al_2O_3 while cryolite alone dissolves only 15.7 wt. % Al_2O_3.

In sections (d), (e), and (f), Figure 2, cryolite precipitates as the primary phase on the low alumina side of the double saturation minimum. At higher alumina contents, the primary phase is β-Al_2O_3. The slopes of the alumina liquidus reverse the previous trend and increase with increasing sodium fluoride content.

In section (g), Figure 2, sodium fluoride rather than cryolite precipitates as the primary phase on the low alumina side of the double saturation minimum. β-alumina is the first crystal that forms from melts on the high alumina side.

With sections (f) [40 wt. % NaF] and (g) [42 wt. % NaF] cutting across the cryolite and sodium fluoride phase fields respectively, the following melt compositions were investi-

Table I. Composition Points and Related Primary Phases Used to Define the α-, β-Al_2O_3 Univariant Line

Composition (Wt. %)			Primary Phase
NaF	Al_2O_3	Na_3AlF_6	
7.0	11.0	82.0	α-Al_2O_3
8.0	11.0	81.0	β-Al_2O_3
7.5	12.0	80.5	α-Al_2O_3
8.8	12.0	79.2	β-Al_2O_3
13.5	16.0	70.5	α-Al_2O_3
15.0	16.0	69.0	β-Al_2O_3

gated to locate the cryolite–sodium fluoride univariant line: 41 wt. % NaF, 1 wt. % Al_2O_3, 58 wt. % Na_3AlF_6 and 41 wt. % NaF, 2 wt. % Al_2O_3, 57 wt. % Na_3AlF_6. The first of these compositions precipitated NaF and Na_3AlF_6 simultaneously, and therefore, was judged to be located on the ternary univariant line. The second composition precipitates sodium fluoride as the primary phase. These two melt compositions and others located on sections (f) and (g) were triply saturated with respect to NaF, Na_3AlF_6 and β-Al_2O_3 at 880° C. The ternary eutectic was determined by a short extrapolation of univariant lines to occur at 881° C. with a composition of 40.5 wt. % NaF, 2.3 wt. % Al_2O_3, and 57.2 wt. % Na_3AlF_6. The phase fields thereby defined are shown in Figure 3.

The ternary weight compositions of Figures 1, 2, 3 and Table I were converted to Na_6F_6, Al_2F_6, Al_2O_3 reciprocal molar quantities. The appropriate liquidus temperatures were then utilized in plotting Figure 4.

The univariant line which separates the NaF and β-Al_2O_3 phase fields was obtained by determining the primary phase for a number of compositions in that area. This line extends from E (Figure 4) towards the sodium fluoride-rich corner of the diagram, where it joins the NaF–$NaAlO_2$ and β-Al_2O_3–$NaAlO_2$ univariant lines at an invariant reaction point (P_1). Liquidus temperatures, however, were not determined because of the steepness of the sodium aluminate and β-alumina surfaces. The composition of the peritectic, P_1, (92.1 mole % Na_6F_6, 5.5 mole % Al_2F_6, 2.4 mole % Al_2O_3) differed slightly from the theoretical composition (92.7 mole % Na_6F_6, 3.4 mole % Al_2F_6, 3.8 mole % Al_2O_3) which was based on secondary crystallization temperature of NaF–Al_2O_3 melts (*8*). The agreement, however, is good in view of the assumptions made in the theoretical calculations.

Table II summarizes data concerning composition, temperature, and the equilibrium solid phases for the various eutectic and peritectic points. The compositions of e_3 and e_4 were taken from the work of DePable-Galan (*5*).

The univariant line separating the sodium aluminate and β-alumina phase fields, starting at P_1, is extrapolated to join the eutectic of these same two compounds on the Na_6O_3–Al_2O_3 axis at e_3. Similarly, the univariant that defines the α-Al_2O_3 and β-Al_2O_3 double saturation state starting at P_2, is extended to contact the binary eutectic at e_4. Interestingly, the region of maximum alumina solubility, as indicated by the humps in the isotherms, follows the penetration of the α-, β-Al_2O_3 univariant into the diagram.

CRYOLITE-SODIUM ALUMINATE SECTION

Interest in this system has been demonstrated by the appearance of several publications within the past decade dealing with liquidus temperatures (*3*), structural evaluations based on liquidus temperatures in cryolite-rich melts (*10*) and the identification of sub-liquidus sintered products (*1*).

The phase relationships for addition of sodium aluminate to cryolite can be derived from Figure 4 and compared to earlier findings. Consider compositions along the line joining the cryolite (Na_6F_6/Al_2F_6 = 1) and the sodium aluminate ($Na_{3.2}Al_{3.2}O_3$) points for which liquidus temperatures are available. Figure 5 shows the vertical section for this system. The liquidus temperatures reported by Holm's (*10*) for compositions up to 6 mole % sodium aluminate are shown to agree with those taken from Figure 4. Bonnier (*3*) employed the thermal arrest method with fast cooling rates (10°/min.) and reports a eutectic at 49.8 mole % $NaAlO_2$ and 897° C. The minimum in the liquidus curve of Figure 5 occurs at 23.5 mole % sodium aluminate and 951°. This minimum cannot be interpreted as a eutectic because the cryolite–sodium aluminate join is neither a "true" nor a "quasi" binary system. The reason being that the composition of the primary phase forming from the melt beyond the minimum is not located on the join. Compositions located between the cryolite vertex and the minimum precipitates cryolite as primary phase. The composition of the liquid phase follows the liquidus curve on further cooling until β-Al_2O_3 forms from the melt at 951° C. A condition of univariant equilibrium is attained at this temperature. So that, on further cooling, the composition of the liquid phase departs from the cryolite–sodium aluminate join (Figure 5) and moves in the direction of E (Figure 4) along the line P_2 – E where the final products of crystallization are realized at 881° C. Somewhat differently, however, the composition of the liquid phase to the right of the liquidus minimum of Figure 5 departs immediately from the join on the appearance of primary phase β-Al_2O_3. The cryolite, β-alumina double saturation line is encountered at successively lower temperatures for starting compositions increasing is sodium aluminate content. These compositions, like all those located in conjugate sub-system II (Figure 4), ultimately became triply saturated with respect to sodium fluoride, cryolite and β-alumina at the invariant point E.

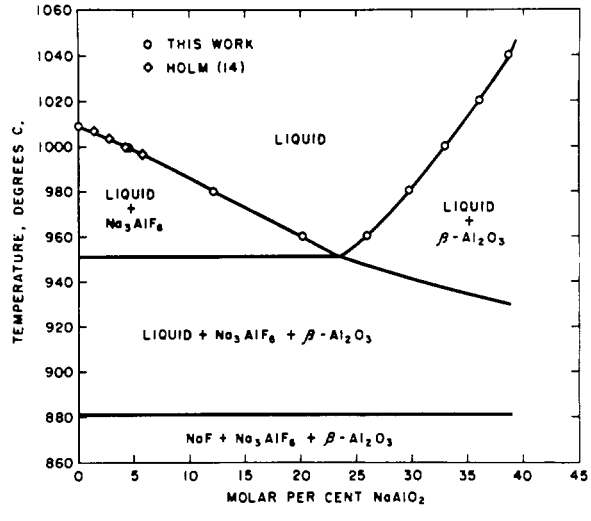

Figure 5. The Na_3AlF_6–$NaAlO_2$ section at the Na_6F_6–Al_2F_6–Na_6O_3–Al_2O_3 reciprocal section

Table II. Invariant Compositions, Temperatures and Related Equilibrium Solid Phases

Point	Composition, % Na_6F_6	% Al_2F_6	% Al_2O_3	% Na_6O_3	Temp., °C.	Solid Phases
e_1	68.4	31.6	...	...	888	Na_3AlF_6, NaF
e_2	40.3	40.3	19.4	...	961	Na_3AlF_6, Al_2O_3
e_3	...	...	87.5	12.5	...	$NaAlO_2$, β-Al_2O_3
e_4	...	...	98.3	1.7	...	β-Al_2O_3, α-Al_2O_3
P_1	92.1	5.5	2.4	...	985	$NaAlO_2$, β-Al_2O_3, NaF
P_2	43.2	38.2	18.6	...	956	Na_3AlF_6, β-Al_2O_3, α-Al_2O_3
E	65.2	29.8	5.0	...	881	Na_3AlF_6, B-Al_2O_3, NaF

LITERATURE CITED

(1) Albert, O., Breit, H., *Aluminium Ranshofen Mitt.* **3**, 3 (1955).
(2) Arakelyan, O.I., *Tsvetn. Metal.* **34**, No. 10, 64 (1961).
(3) Bonnier, E., *Ann. Phys.* **8**, 259 (1953).
(4) Brynestad, J., Grjotheim, K., Grönvold, F., Holm, J.L., Urnes, S., *Discussions Faraday Soc.* **32**, 90 (1961).
(5) DePablo-Galan, J., Foster, W.R., *J. Am. Ceram. Soc.* **42**, 491 (1959).
(6) Foster, P.A., Jr., *J. Electrochem. Soc.* **106**, 971 (1959).
(7) Foster, P.A., Jr., *J. Am. Ceram. Soc.* **43**, 66 (1960).
(8) *Ibid.*, **45**, 145 (1962).
(9) Ginsberg, H., Resch, K., *Z. Erzbergbau Metallhuettenw.* **15**, 199 (1962).
(10) Holm, J.L., *Trans. Faraday Soc.* **58**, 1104 (1962).
(11) Kostjukov, A.A., cited by A.I. Beljajew, "Metallurgie des Aluminiums," Vol. I, VEB Verlag Technik, Berlin, 1956.
(12) Pazukhin, V.A., Izv. *Vysshikh Uchebn. Zavedenii, Tsvetn. Met.* No., 71 (1958).
(13) Phillips, N.W.F., Singleton, R.H., Hollingshead, E.A., *J. Electrochem. Soc.* **102**. 690 (1955).
(14) Rolin, M., *Bull. Soc. Chim. France* **1960**, 1201.

RECEIVED for review June 29, 1963. Accepted December 23, 1963.

Solid Compound Formation in the CCl_4 Mixtures of p-Dioxane with CCl_4, $CBrCl_3$, and $CFCl_3$. Solid-Liquid Phase Equilibria in Binary and $CFCl_3$ Systems

J. B. OTT, J. R. GOATES, and N. F. MANGELSON
Brigham Young University, Provo, Utah

Solid-liquid phase diagrams have been obtained from time-temperature cooling curves for the three binary systems formed from p-dioxane with CCl_4, $CFCl_3$, and $CBrCl_3$. Solid compounds with the empirical formulas of $p\text{-}C_4H_8O_2\cdot(CCl_4)_2$ and $p\text{-}C_4H_8O_2\cdot(CFCl_3)_2$ were formed. The system $p\text{-}C_4H_8O_2$–$CBrCl_3$ shows a maximum freezing point in a solid solution, but the evidence is against compound formation in that system. Exploratory measurements on the CH_3CCl_3–dioxane and $(CH_3)_3CCl$–dioxane systems show that they do not form compounds. These results are in qualitative agreement with the concept that p-dioxane is acting as an electron donor and the halogenated molecules as acceptors in the intermolecular compounds.

PREVIOUS PHASE DIAGRAM studies have shown that CCl_4 forms solid compounds with benzene and several of its derivatives (*2, 3, 6, 7, 9, 11, 12*). Each of the aromatic substances that is known to form the CCl_4 addition compound is characterized by a high electron density in the benzene ring, which suggests that the aromatic compound acts as a donor in a charge-transfer process. This explanation is supported by x-ray diffraction work on the related CBr_4-*p*-Xylene system (*13*).

Other molecules capable of acting as electron donors might also form compounds with CCl_4. Dioxane appears to meet the requirements for a donor molecule; and it is known to form a compound with CCl_4 (*8*).

This paper reports a solid-liquid phase equilibria study of *p*-dioxane with CCl_4 (a more detailed study than the earlier work referred to above), $CBrCl_3$, and $CFCl_3$. The selection of the three halogen compounds, all of roughly the same shape and size, made possible a study of the effect of electronegativity of a substituent atom in CCl_4 on the ability to form the intermolecular compound.

EXPERIMENTAL

Chemicals. Starting materials were spectro-grade *p*-dioxane and reagent grade CCl_4, $CBrCl_3$, and $CFCl_3$. The dioxane, CCl_4, and $CFCl_3$ were purified by fractional distillation in a vacuum-jacketed 100-cm. column packed with glass helices and operated at a reflux ratio of approximately 50:1. The $CBrCl_3$, because it showed signs of some decomposition (yellow color) under the conditions that the other substances were distilled, was vacuum distilled at room temperature in a 170-cm. long, glass helices packed distillation column and then fractionally crystallized once. The entire distillation apparatus was shielded from light by wrapping it in aluminum foil, since there was evidence for photchemical as well as thermal decomposition of this material.

With the exception of the $CBrCl_3$, which is discussed below, the purity of the products was determined from their time-temperature freezing curves. Calculations of the change in melting point as a function of the fraction melted showed the following liquid soluble-solid insoluble impurities present: *p*-dioxane, 0.06 mole %; CCl_4, 0.02 mole %; and $CFCl_3$, 0.05 mole %. The CH_3CCl_3 and $(CH_3)_3CCl$ used in the exploratory measurements were also purified by fractional distillation.

Because of the physical properties of the $CBrCl_3$ (hard and massive crystals and small heat of fusion), it was difficult to obtain equilibrium conditions between solid and liquid, and the freezing curve for this substance was